Materials Science & Engineering A 833 (2022) 142520

Contents lists available at ScienceDirect

Materials Science & Engineering A

journal homepage: www.elsevier.com/locate/msea

Study on the micro-interface behavior of 2024Al light alloy bonded by ultrasonic assisted solid phase diffusion welding with Ag interlayer under atmosphere

Qian Wang [a,d,*], Yong Nie [d], Yingfeng Shao [b], Hongzhi Liu [c], Xiaoqiang Hu [a,e], Dianzhong Li [a,e]

[a] Ganjiang Innovation Academy, Chinese Academy of Sciences, Ganzhou, 341000, People's Republic of China
[b] State Key Laboratory of Nonlinear Mechanics and Beijing Key Laboratory of Engineered Construction and Mechanobiology, Institute of Mechanics, Chinese Academy of Sciences, Beijing, 100190, China
[c] Institute of Electronic Engineering, China Academy of Engineering Physics, Mianyang, 621999, China
[d] School of Materials Science and Engineering, Tianjin University of Technology, Tianjin, 300384, China
[e] Shenyang National Laboratory of Materials Science, Institute of Metal Research, Chinese Academy of Sciences, Shenyang, 110016, PR China

ARTICLE INFO

Keywords:
Ultrasound
Solid phase welding
Plastic deformation
Amorphous
Intermetallic compound

ABSTRACT

This paper introduces a new welding process. Based on the traditional solid phase diffusion welding, the ultrasonic energy field is introduced, and the acoustic plastic effect caused by ultrasonic vibration propagating in the solid phase medium is used to promote the plastic deformation of the base metal, so as to form an effective joining. Combined with the model analysis, the theory proves that the introduction of ultrasonic energy field can reduce the welding pressure and shorten the welding time. The plastic deformation was confirmed by the observation of dislocation and twinning in the weld seam with Ag as intermediate layer in atmospheric environment. The maximum shear strength of the welded joint is about 84.33 MPa. It was also found that the oxide Ag2O can help compounds with different crystal structures form bonds.

1. Introduction

With the continuous development of the field of electronic packaging, silicon carbide and nitride are introduced into electronic devices so that they can operate continuously at temperatures above 350 °C [1,2]. The Cu substrate commonly used in electronic devices appears to be delaminated in practical applications and cannot further meet the use conditions [3,4].

Aluminium alloys are among the most widely used lightweight alloys. They have been widely used in automotive and aerospace fields [5–8]. Additionally, they are used in the radiators of automobiles because of their excellent thermal stability. It was reported that 1500 thermal cycles between -55 °C and ~250 °C were conducted on an aluminium alloy. Cracks and delamination were not observed for the aluminium alloy in the experiment, and thus, the alloy can be used as a substrate instead of Cu in electronic packaging [9]. Therefore, it is necessary to develop a new process to connect aluminium alloys.

Traditional solid phase diffusion welding technology can reduce the formation of joint defects such as deformation, cracking and segregation [10,11]. This process relies on the application of high pressures for long times to promote microplastic deformation of the surface of the material to be welded, and elemental forms a close joining. At present, relevant research reports show that ultrasonic softening in solid media can promote the plastic deformation of materials [12,13]. Therefore, a new welding process is designed in this paper, which introduces ultrasonic energy field on the basis of traditional solid phase diffusion welding. The acoustic plastic effect caused by the propagation of ultrasonic vibration in solid medium is used to promote the plastic deformation of base metal, accelerate the mutual diffusion of elements, form effective metallurgical bond, shorten welding time, improve welding efficiency and reduce welding cost.

In this paper, a 2024 light aluminium alloy was connected by ultrasonic assisted solid phase diffusion welding with Ag foil as the intermediate layer. The effects of different ultrasonication times on the microstructure and mechanical properties were studied. The effect of ultrasound on the contact interface between the base metal and interlayer was studied. Effects of ultrasonication on plastic deformation between the base metal and interlayer were evaluated.

* Corresponding author. Ganjiang Innovation Academy, Chinese Academy of Sciences, Ganzhou, 341000, China.
E-mail address: qianwang@gia.cas.cn (Q. Wang).

https://doi.org/10.1016/j.msea.2021.142520
Received 19 October 2021; Received in revised form 14 December 2021; Accepted 15 December 2021
Available online 17 December 2021

Table 1
2024Al chemical composition table.

Element	Fe	Cu	Mn	Mg	Cr	Zn	Al
Content	0.5	3.8–4.9	0.3–1.0	1.2–1.8	0.1	0.25	Bal.

2. Experimental procedures

2.1. Materials

In this paper, 2024 Al with shear strength of 285 MPa and 99% Ag foil with thickness of 0.05 mm were purchased from the market. The chemical composition parameters are shown in Table 1. The 2024 Al sample with the size of 10 mm × 10 mm x 5 mm was used as the base metal, and the Ag foil was made of 10 mm × 10 mm x 0.05 mm as the interlayer. The base metal was grinded on 400 #, 800 #, 1500 #, 2000 # water sandpaper in turn, and the contact surface was polished into mirror by 1 um Al_2O_3 polishing agent. The polished base metal and interlayer were placed in anhydrous ethanol for ultrasonic cleaning for 15 min and then dried and placed in a vacuum dryer for standby.

2.2. Soldering process

As shown in Fig. 1 (a), a self-assembly set of ultrasonic-assisted welding system equipment is used in the welding process, which is equipped with an ultrasonic generator, muffle furnace induction heating device and a circulating cooling system. Place the sample in the muffle furnace heating device in the form of 2024Al/Ag/2024Al sandwich. The ultrasonic probe was placed on the upper surface of 2024Al in the sandwich structure, and a constant pressure of 0.1 MPa was applied. Two K-type thermocouples were placed to detect the welding temperature. Raise the temperature to 500 °C, apply ultrasonic vibration time 20 s, 35 s, 50 s, 65 s. After the ultrasonic treatment, the upper surface pressure was maintained at 0.1 MPa until the sample was cooled to room

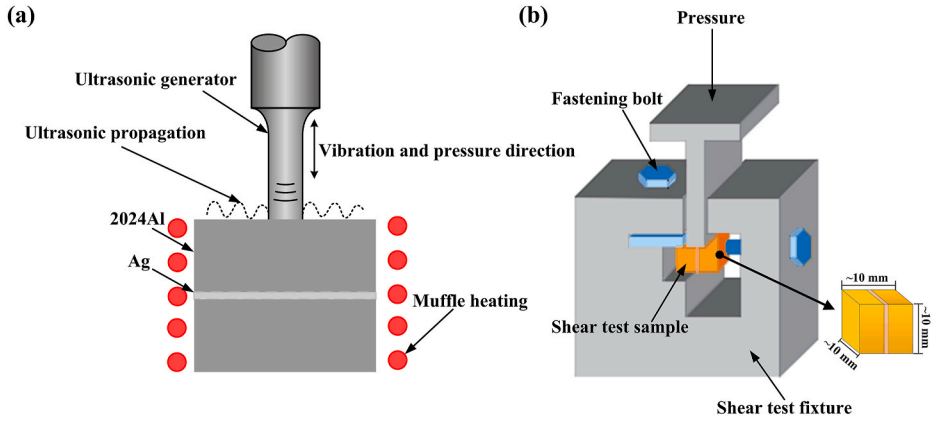

Fig. 1. (a) Welding process diagram; (b) Shear test schematic.

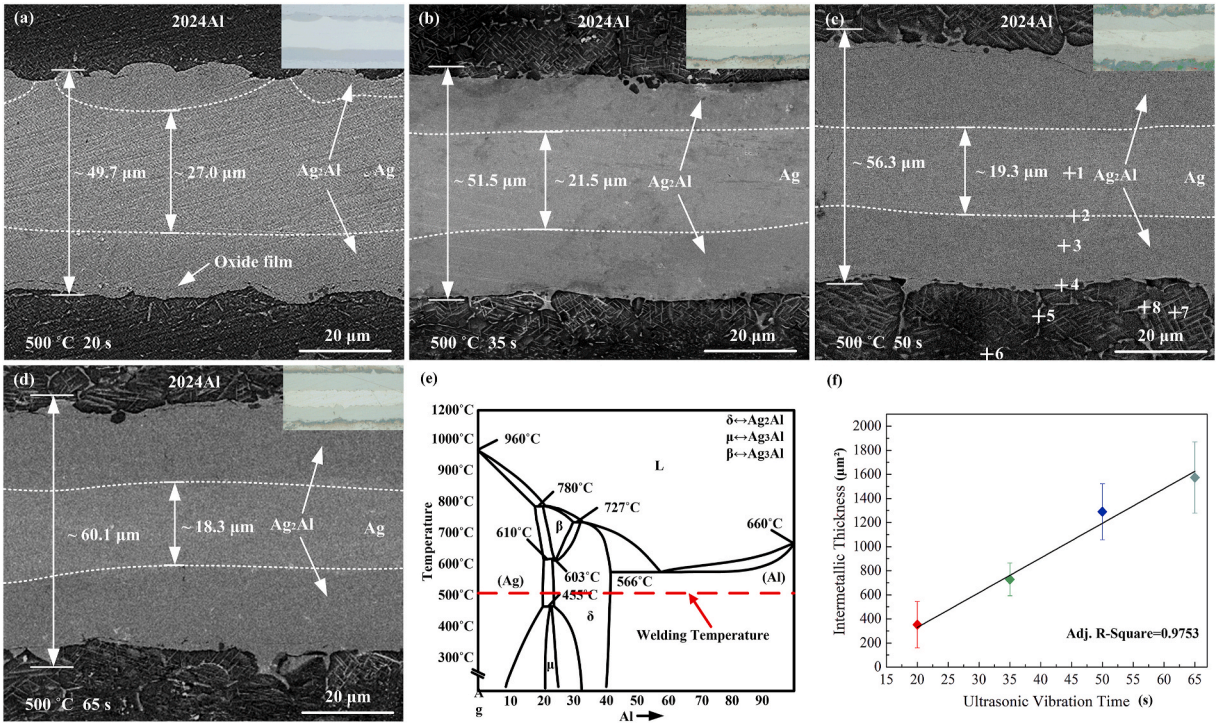

Fig. 2. Microstructure of the joint obtained by different ultrasonic vibration time: (a) ultrasonic vibration for 20 s; (b) ultrasonic vibration for 35 s; (c) ultrasonic vibration for 50 s; (d) ultrasonic vibration for 65 s; (e) al-ag binary phase diagram and (f) intermetallic compound thickness and ultrasonic time fitting diagram.

Table 2
Element composition at different positions of the joint obtained by ultrasonic vibration for 20 s.

	Al(at%)	Ag(at%)	Possible phase
Point 1	3.85	96.15	Ag
Point 2	4.02	95.98	(Ag)
Point 3	39.5	60.5	Ag_2Al
Point 4	66.07	33.93	(Al)+ Ag_2Al
Point 5	94.61	5.39	(Al)
Point 6	100	0	Al
Point 7	88.14	11.86	(Al)
Point 8	41.38	58.62	Ag_2Al+(Al)

temperature, and the sample was taken out under unloading pressure.

2.3. Characterization and observations

The microstructure of the sample weld was observed under a scanning electron microscope (SEM, ZEISS MERLIN Compact and S-3400), and the energy spectrum analysis of the microstructure and composition was performed. The transmission samples were prepared by Fast Fourier Transformation (FIB) and observed under high-resolution transmission electron microscopy (HRTEM, Talos F200X). The strength was measured by a WDW-D100EIII micro electronic universal testing machine at a constant speed of 0.5 mm/min at 250 °C. The schematic diagram of the strength test process is shown in Fig. 1 (b). Test at least three times under each test condition. The fracture surface morphology was detected by SEM.

3. Experimental results

Fig. 2 (a) - (d) show the microstructure of the joint obtained at 500 °C for different ultrasonic vibration times. No obvious defects, such as cracks and holes, were observed around the weld.

Fig. 2 (a) shows that when the ultrasonic vibration time was 20 s, a grey phase formed on both sides of the reaction interface, and its thickness was uneven and discontinuous. The grey phase on one side of the intermediate Ag layer was less than that on the other side, and the total thickness of the grey phases on both sides was approximately 22.7 μm on average. On the Al side of the upper and lower interfaces, a grey-white needle-like material appeared.

Fig. 2 (b) shows the microstructure of the joint after ultrasonic vibration for 35 s. The grey phase continued to grow along the reaction interface, and the total thickness of the grey phase on both sides averaged approximately 30 μm. The grey phase thickness on both sides of the upper and lower reaction interface was uniform, and the weld width became wider. The thickness of the intermediate layer Ag decreased and was gradually consumed by the reaction. The greyish-white needles on the 2024Al side of the upper and lower interfaces gradually increased.

Fig. 2 (c)–(d) show the microstructures of the joints obtained by applying ultrasonic vibration for 50 s and 65 s, respectively. The thickness of the grey phase formed at the reaction interface continued to increase, and the average sum of the grey phase thicknesses on both sides was 37 μm and 41.8 μm. The grey phase thickness on both sides of the reaction interface tended to be average, the overall width of the weld continued to increase, and the intermediate Ag layer gradually decreased with increasing ultrasonic vibration time. The distribution of grey-white acicular matter on both sides of Al continued to increase.

As shown in Fig. 2 (c), 8 points at different locations were selected for EDS elemental analysis of the composition of the grey phase. Elemental analysis results are shown in Table 2. The atomic percentages of Al and Ag at point 3 are approximately 2:3. According to the Al–Ag binary phase diagram in Fig. 2 (e) and the relative valency effect in the Hume-Rothery principle, the solubilities of the high-valence component and low-valence component differ, and as a result, Ag and Al cannot form a continuous solid solution at the welding temperature of 500 °C [14]. When the atomic percentage of Al is approximately from 23 at% to 40 at %, Ag_2Al with a hexagonal structure precipitates in the matrix. Thus, the grey intermetallic compound at point 3 is Ag_2Al [15].

Fig. 3 shows the microstructure of the grey-white needle-like material on the 2024Al side of the joint obtained at 500 °C for different ultrasonic vibration times. Fig. 3 (a) shows the microstructure of the grey-white matter on the 2024Al side of the welded joint obtained by ultrasonic vibration for 20 s. The figure shows that the diffusion thickness of the grey-white needles is approximately 4.9 μm, and the grey-white needles are chaotic.

Fig. 3 (b) shows the microstructure of the grey-white matter on the 2024Al side of the welded joint obtained by ultrasonic vibration for 35 s. The figure shows that the diffusion thickness of the grey-white needles increased with increasing ultrasonic vibration time, and the diffusion layer thickness was approximately 12.9 μm. The number of grey-white needles increased, and the distribution was more uniform. Many grey-

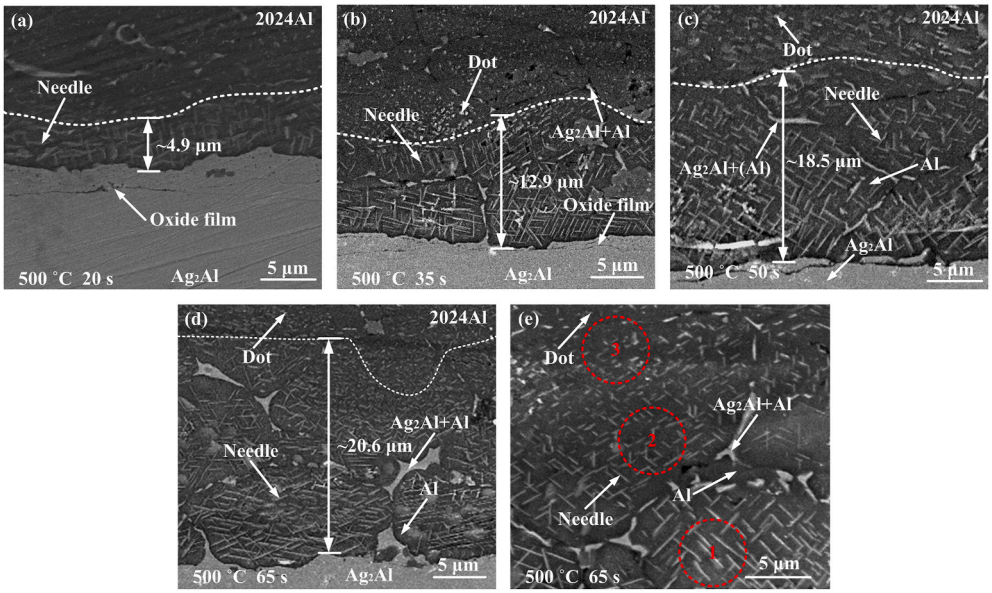

Fig. 3. The morphology of grey-white matter in the welded joint under different ultrasonic vibration time: (a) Ultrasonic vibration for 20 s; (b) Ultrasonic vibration for 35s; (c) Ultrasonic vibration for 50s; (d) Ultrasonic vibration for 65s; (e) 65 s local expansion diagram of ultrasonic vibration.

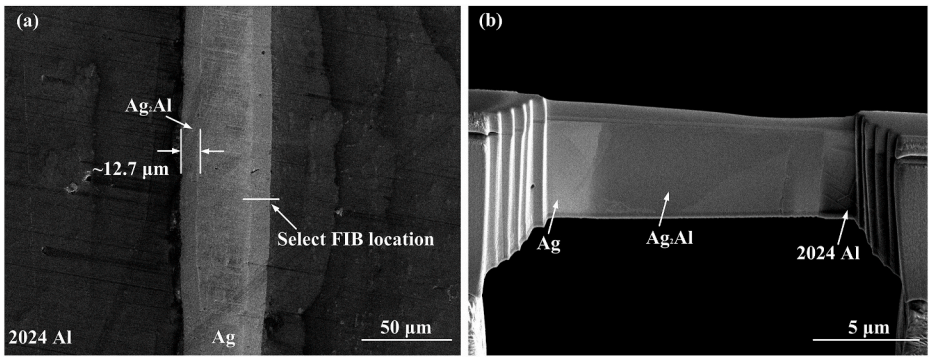

Fig. 4. (a) FIB sample selection diagram; (b) Transmission sample diagram.

white dots were observed far from the reaction interface. With ultrasonic vibration, the base metal 2024Al gradually changed from a single block to several ellipsoids, and the grey phase filled the gaps between the ellipsoids. According to the EDS data at point 8 in Table 2, the grey phase in the gaps between the ellipsoids was Ag_2Al+(Al). According to elemental analysis, Ag_2Al+(Al) is precipitated from the Al grain boundary of the base metal.

Fig. 3 (c)–(d) show the microstructure of the grey-white matter on the side of the 2024Al welded joints obtained by ultrasonic vibration for 50 s and 65 s. The figures showed that with increasing ultrasonic vibration time, the thickness of the grey-white needle-like diffusion layer increased, and the number of needles also increased. With increasing ultrasonic vibration time, the amount of grey-white dot-like material increased and dispersed in the ellipsoidal blocks of 2024Al. The amount of 2024Al in the ellipsoidal blocks increased gradually.

Fig. 3 (e) shows the local amplification of the grey-white material in the diffusion layer in the joint obtained by ultrasonic vibration for 65 s. According to the figure, there were three different forms of grey-white matter in the red circle. The No. 1 red circular frame was close to the reaction interface, and the grey-white matter in the frame was needle-like, with an average length of approximately 2.5 μm. Most of the grey-white acicular matter intersected and was distributed in a disorderly manner. The No. 2 red round frame was located a short distance from the reaction interface, and the grey-white substance in the frame was needle-like, with an average length of approximately 1.1 μm. The distribution of grey-white acicular matter was chaotic. Compared with the grey-white needles in red round frame No. 1, the grey-white needles gradually decreased in size with distance from the reaction interface. The No. 3 red round frame was located far from the reaction interface, and the grey and white matter in the box was dotted with an average length of less than 0.2 μm. The grey-white dots were dispersed in the ellipsoidal blocks of Al, which separated from the Al matrix. According to the morphological transformation process of the grey-white matter, with increasing distance from the reaction interface, the diffusion of the grey-white matter gradually decreased from grey-white needles with an average length of 2.5 μm to grey-white dots with an average length of less than 0.2 μm, until it completely disappeared.

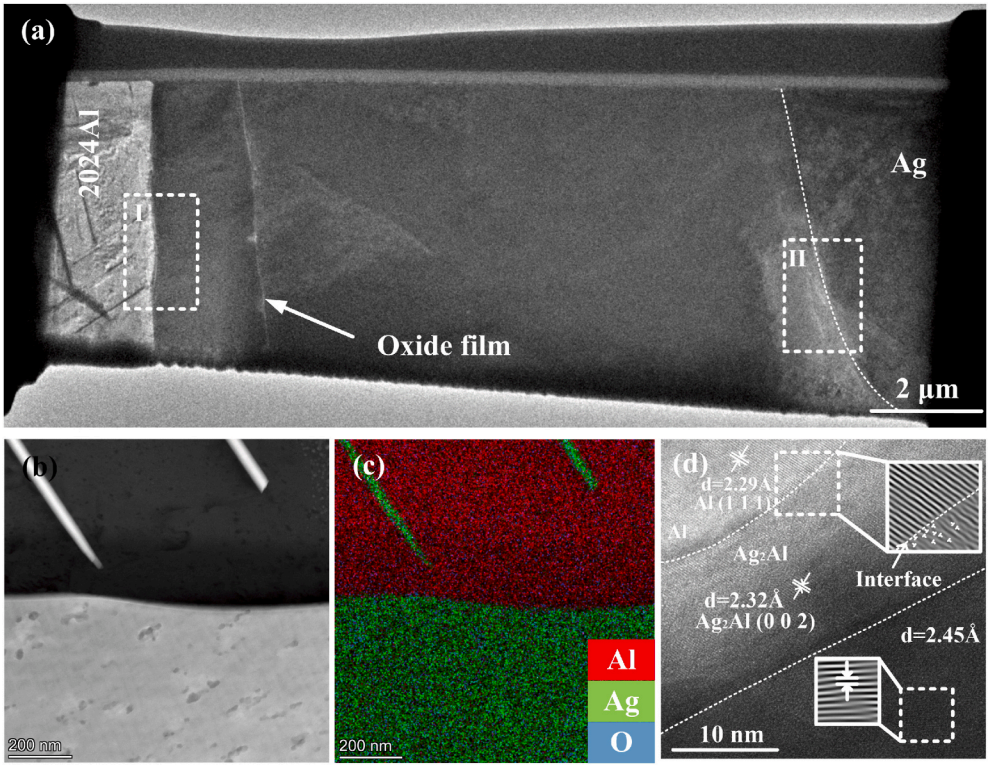

Fig. 5. TEM morphology of (a) joint of Al/Ag/Al joint by ultrasonic assisted solid phase diffusion welding; (b) Interface morphology between 2024Al and the product; (c) is the EDS detection diagram at the interface; (d) HRTEM image of the interface between 2024Al and the product.

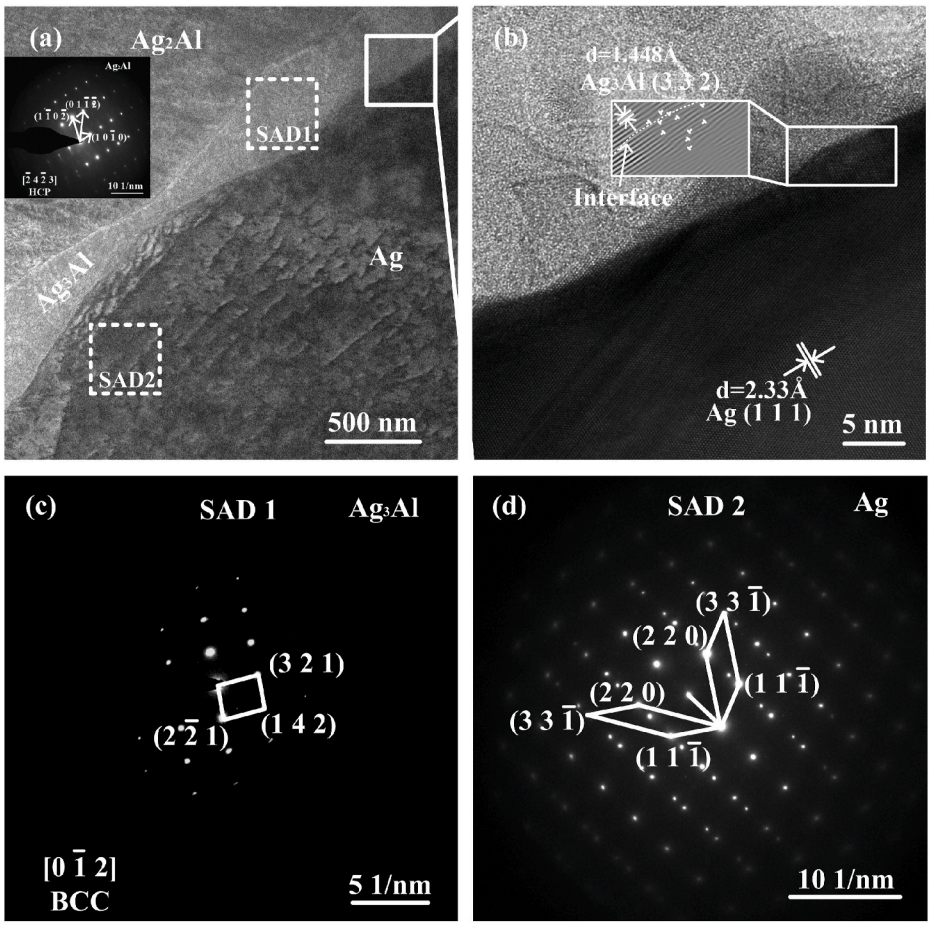

Fig. 6. Shows the (a) morphology of the region II at the intermediate layer Ag and the producer interface in Fig. 5; (b) Interface HRTEM image; (c) SAD1 electron diffraction pattern; (d) SAD2 electron diffraction pattern.

4. Discussion

A linear fit was performed to analyse the variation of the thickness of the intermetallic layer of Ag_2Al with the applied ultrasonication time in an atmospheric environment. The results showed that the square of the thickness of the layer of the intermetallic compound Ag_2Al was linearly proportional to the ultrasonication time, and the regression coefficient was 0.9753, as shown in Fig. 2 (f).

The linear relationship can be expressed as [16]:

$$I_{Ag_2Al}^2 = D_{Ag}^{'} t \tag{1}$$

where I_{Ag2Al} in the formula is the thickness of the layer of the intermetallic compound Ag_2Al; $D_{Ag}^{'}$ is the diffusion coefficient of elemental Ag in elemental Al under ultrasonic vibration; and t represents the time that an ultrasonic vibration is applied.

The measured data in Fig. 2 (a)–(d) were substituted into the formula, and the mutual diffusion coefficient $D_{Ag}^{'} = 2.88\times10^{-7}\ cm^2/s$ between Ag and Al under ultrasonic vibration was calculated according to the fitting results. Without ultrasonic vibration, the mutual diffusion coefficient of Ag and Al is $D_{Ag} = 6.6\times10^{-9}\ cm^2/s$ [17]. Comparing the diffusion coefficients of the two elements showed that ultrasonication can increase the mutual diffusion coefficients of Ag and Al by approximately two orders of magnitude. This indicates that ultrasonic vibration can promote atomic diffusion at the solid interface.

To further analyse the reaction at the interface, a sample that underwent ultrasonic vibration for 20 s was selected for FIB to prepare the transmission sample. The position shown in Fig. 4 (a) was selected to prepare TEM samples. The figure showed that the thickness of the intermetallic compound Ag_2Al was approximately 12.7 μm. Therefore, the length of the region selected for the TEM sample was approximately 14.4 μm. The sample contained base metal, intermetallic Ag_2Al and an intermediate layer. In Fig. 4 (b), there is grey intermetallic Ag_2Al, and a lesser amount of a light grey phase that is not detected by SEM and EDS.

Fig. 5 shows the HRTEM and EDS of the Al/Ag/Al joint formed by ultrasonic assisted solid phase diffusion welding. Fig. 6(a) shows that the selected positions can be divided into three parts, namely, base metal 2024Al, product and Ag in the intermediate layer. There was a small number of needles in 2024Al. Fig. 5 (b)–(c) show the microscopic morphology and EDS diagram at the interface between 2024Al and the product. The needles were mainly composed of Ag and a small amount of Al. As shown in Fig. 5 (d), region I at the interface between 2024Al and the product was selected for high-resolution analysis. Fig. 5 (d) shows that there are two parts of the phase in region I, namely, Al and the intermetallic compound Ag_2Al.

A fast Fourier transform (FFT) was performed at the interface between Al and intermetallic Ag_2Al. It can be observed from the FFT diagram that there were many dislocations at the interface, mainly distributed on the Ag_2Al side, and no obvious dislocations were found on the Al side. Observations prove that slip occurred at the interface, and the material underwent plastic deformation. Dislocations were concentrated on the side of the generated intermetallic compound Ag_2Al, while no obvious dislocations were found on the side of 2024 Al. This phenomenon occurred because the stacking fault energies of various types of phases differed, resulting in various regions of dislocations. A phase with small stacking fault energy is more prone to dislocation accumulation or disorderly distribution [18]. The stacking fault energy of Al is 166 mJ/m^2, while that of the intermetallic compound Ag_2Al is

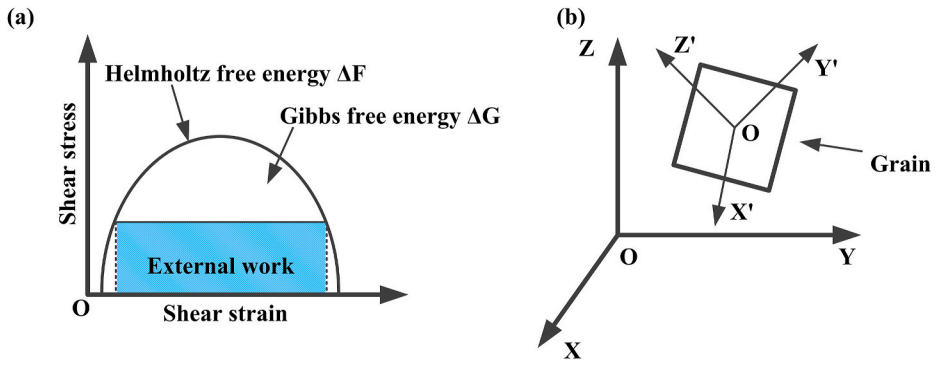

Fig. 7. The relationship between Helmholtz free energy and external work, Gibbs free energy [23]; Diagram of grain angle [25].

approximately 85~87 mJ/m^2 [19]. The stacking fault energy of the intermetallic compound Ag_2Al was smaller than that of Al, so the dislocations were mainly distributed on the side of Ag_2Al.

Fig. 6 shows an HRTEM image and electron diffraction patterns of region II at the intermediate layer Ag and the product interface in Fig. 5. Fig. 6 (a) shows an HRTEM image of region II of the intermediate layer of Ag and the product interface. The figure shows that there were three phases in the interface, and electron diffraction measurement was carried out in the region where the three phases were located. From the inset in Fig. 6 (a), it was determined that the phase in the upper left corner is the intermetallic compound Ag_2Al. The lower right corner phase is the intermediate layer Ag. Fig. 6 (c) shows the electron diffraction pattern of the transition phase between the intermediate layer Ag and intermetallic compound Ag_2Al phase. The calibration showed that the phase was Ag_3Al. Combined with the phase diagram in Fig. 2 (e), at 450 °C, the intermetallic compound Ag_2Al reacted with the intermediate layer Ag to form the intermetallic compound Ag_3Al.

The expression is as follows:

$$Ag_2Al + (Ag) \rightleftharpoons Ag_3Al$$

The expression shows that the inclusion reaction was concentrated on the Ag side of the intermediate layer. Fig. 6 (b) shows an HRTEM image at the interface between the intermediate layer Ag and the generated intermetallic compound Ag_3Al. A fast Fourier transform (FFT) was performed at the interface between Ag and Ag_3Al. The FFT diagram shows that there were many dislocations at the interface, and they were dispersed on the Ag side.

It can be seen from the starting force of dislocation that:

$$\tau_p = \frac{2G}{1-\gamma}\exp\left(-\frac{2\pi\omega}{b}\right) \tag{2}$$

In the formula, τ_p is the critical shear stress; G is the shear modulus; γ is Poisson's ratio; ω is the slip surface spacing; and b is the dislocation Berger vector length.

According to formula 2, the crystal structure of the intermediate layer of Ag was FCC, and the crystal structure of the intermetallic compound Ag_3Al was BCC. Usually, the slip surface spacing ω of face-centred cubic structures is larger than that of body-centred cubic structures, and the calculated critical shear stress of face-centred cubic structures is smaller, so the middle layer of Ag in face-centred cubic structures was more prone to dislocations. According to the previous analysis, when the stacking fault energy is smaller, the material is more prone dislocations. The stacking fault energy of Ag is one of the smallest in known metal materials, and its stacking fault energy is approximately 16~22 mJ/m^2 [20,21]. Therefore, dislocations were more likely to occur in the intermediate layer of Ag than in the intermetallic compound Ag_3Al, resulting in more dislocations on the Ag side than on the Ag_3Al side. Fig. 6 (d) shows the electron diffraction calibration on the Ag side of the intermediate layer. According to the diffraction pattern, twins appeared on the Ag side of the intermediate layer. Usually, because the slip system of dense hexagonal structures is smaller than that of face-centred cubic structures and body-centred cubic structures, dense hexagonal structures do not easily slip. Under large stresses, dense hexagonal structures are more prone to twinning than face-centred cubic structures and body-centred cubic structures. However, no twinning was found in the hexagonal close-packed Ag_2Al. Face-centred cubic structures with small stacking fault energy are prone to twinning, such as austenitic steel [22]. According to the previous analysis, the stacking fault energy of Ag is approximately 16~22 mJ/m^2 and that of Ag_2Al is approximately 85~87 mJ/m^2. The stacking fault energy of Ag_2Al is much larger than that of Ag. Therefore, twins appeared in the face-centred cubic structure of Ag, and no twins appeared in the hexagonal close-packed structure of Ag_2Al. At the same time, the twinning phenomenon observed in the intermediate layer of Ag proved that incomplete dislocation movement occurred at the interface. Combined with the dislocations observed at the interface between Ag_2Al and Al and the interface between Ag_3Al and Ag, plastic deformation occurred at the interface. According to the dislocation rate, the relevant model is established to analyse the influence of ultrasonic vibration on material deformation in solid phase diffusion welding, and the expression is as follows [23]:

$$\dot{\varepsilon} = \dot{\varepsilon_0} exp\left(\frac{-\Delta F}{KT}\right) \tag{3}$$

In the formula, $\dot{\varepsilon}$ is the strain rate; $\dot{\varepsilon_0}$ is a strain constant; k is a Boltzmann constant; T is the absolute temperature; and ΔF is the Helmholtz free energy.

As shown in Fig. 7(a), the Helmholtz free energy can also be expressed as $\Delta F = \Delta G + \Delta W$. In the formula, ΔG is expressed as the change of Gibbs free energy in the system, and ΔW is expressed as the work done by the external environment on the system. When ultrasonic vibration is introduced into solid phase diffusion welding, ΔG and ΔW in the system are reduced, resulting in a decrease in ΔF in the system [23]. According to formula (3), the strain rate of the material is calculated to increase, and the material is more prone to deformation.

Miguel Lagos formulated a theoretical model of diffusion welding, from which can be used to derive an expression relating the interfacial bond rate to the strain rate [24].

$$\lambda = \frac{\dot{A}}{A} = \dot{\varepsilon}\left[-\frac{\pi - 4\theta_c + (1-2\alpha)\sin(4\theta_c)}{\pi\sin(2\theta_c)\left[\cot(2\theta_c) + \alpha\left(2\theta_c - \frac{\pi}{2}\right)\right]}\right] \tag{4}$$

In the formula presented above, $\dot{A}$ represents the area of interfacial bonding, A represents the total area of the surface to be welded, $\dot{\varepsilon}$ represents the strain rate, and θ_c is the angle a grain makes to the z axis before and after diffusion welding, as shown in Fig. 7 (b).

The interfacial bonding rate λ can be used to obtain the time required for welding.

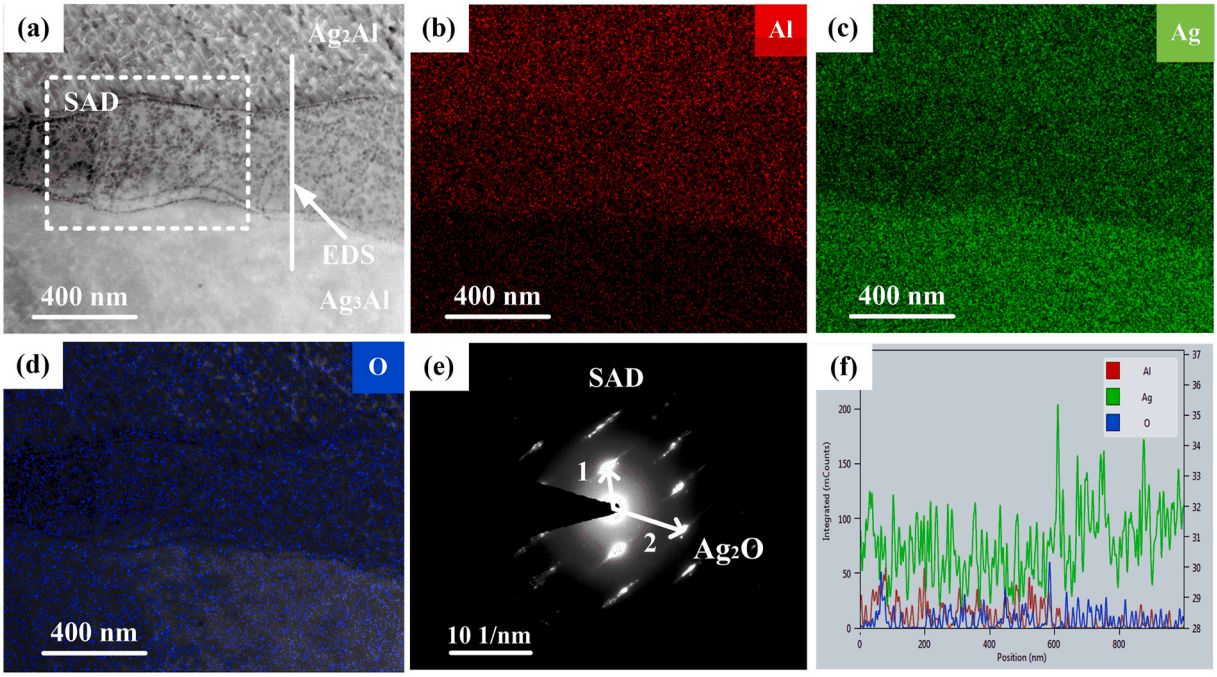

Fig. 8. SEM, EDS and electron diffraction patterns of the interface between the two products.

$$t = \frac{\ln\left(1 - \frac{A}{l^2}\right) d^2}{-\lambda l^2} \tag{5}$$

In the formula presented above, l is the lattice constant and d is the grain size.

Formulas (4)-(5) show that the application of ultrasonication to a solid metal causes the strain rate $\dot{\varepsilon}$ of the material to increase, such that the interfacial bonding rate λ increases. As the interface bonding rate λ is inversely proportional to the welding time t, the welding time t decreases. Therefore, the application of ultrasonication can effectively shorten the welding time.

The Derby model, one of the cavity closure models that has been developed for solid-state welding, describes an initial plastic deformation mechanism, showing that a well-defined plastic deformation is needed for diffusion welding. When the pressure σ' on the joint interface is higher than the yield strength σ_y of the metal, plastic deformation begins [26,27].

The pressure on the interface can be expressed as [26,27].

$$\sigma' = \frac{pa - \gamma}{e} \tag{6}$$

In the formula presented above, γ is the surface energy, p is the pressure of diffusion welding, and e is half the bonding interface length.

The application of ultrasound can reduce the yield strength σ_y of the material, which decreases the σ' required for plastic deformation. In Fig. 2, there is no discernible void in the interface, such that e remains constant. Then, Formula (6) shows that the pressure p required for welding decreases. Therefore, applying ultrasonication can reduce the welding pressure, while maintaining an effective joining at the interface.

It is proven that ultrasonic vibration can lead to plastic deformation of materials. The introduction of an ultrasonic energy field into traditional solid phase diffusion welding can reduce the welding time and pressure parameters.

Fig. 8 (a) shows the morphology of the interface between the intermetallic compounds Ag_2Al and Ag_3Al. The diagram shows that there was

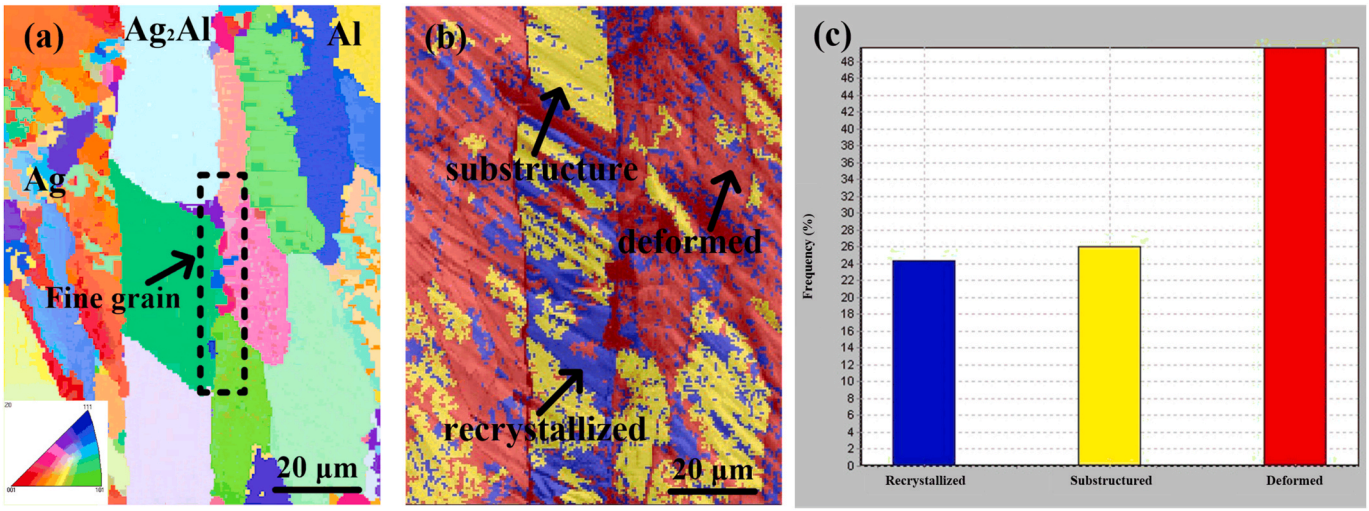

Fig. 9. EBSD diagram of 2024Al–Ag–2024Al joint obtained by ultrasonic assisted solid phase diffusion welding.

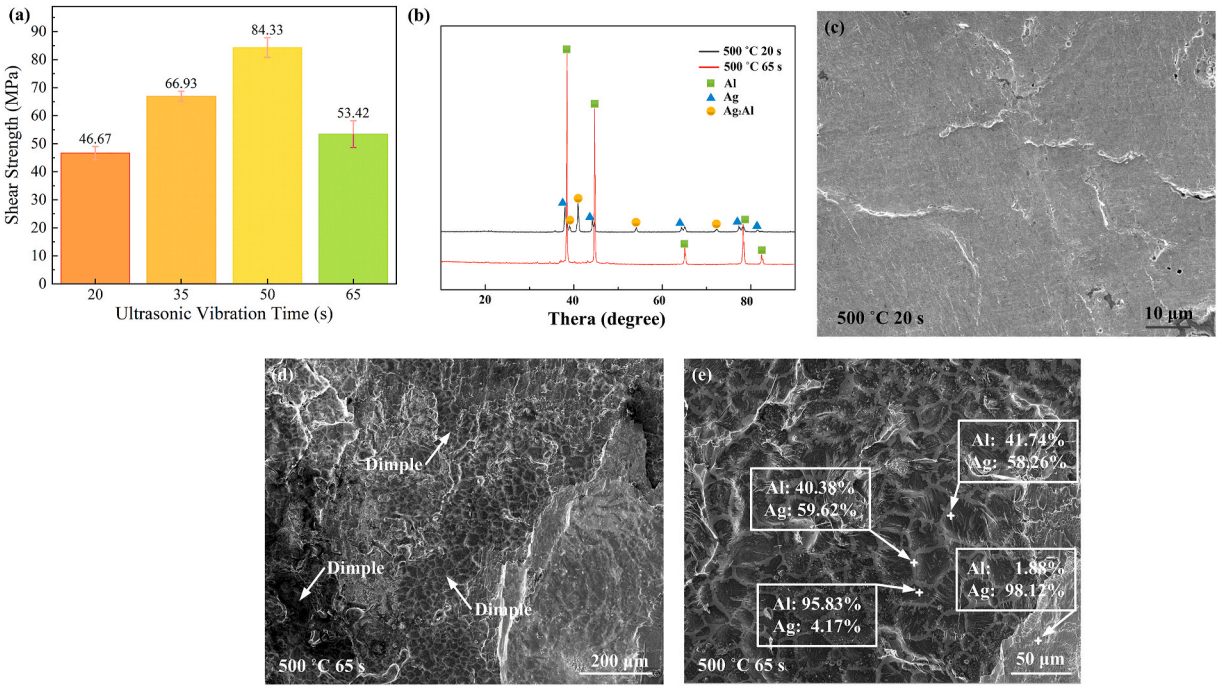

Fig. 10. (a) Shear strength of joints obtained under different ultrasonic time; (b) Ultrasonic vibration for 20 s and 65 s to obtain the fracture of the joint XRD; (c) The fracture morphology of the joint was obtained by ultrasonic vibration for 20 s; (d) The fracture morphology of the joint was obtained by ultrasonic vibration for 65 s; (e) Ultrasonic vibration for 65 s to obtain the amplification diagram of joint fracture morphology.

a transition layer, approximately 333.3 nm thick, between the two intermetallic compounds. Fig. 8 (b)–(d) shows that Al and Ag were evenly distributed, and O was mainly distributed in the excess layer. The diffraction pattern analysis at the transition layer is shown in Fig. 8 (e). According to the diffraction pattern, there were amorphous diffraction rings and diffraction spots around the amorphous diffraction rings in the transition layer. R1 = 2.3 nm corresponds to the (2 0 0) crystal plane of Ag_2O, and R2 = 1.4 nm corresponds to the (3 1 1) crystal plane of Ag_2O. It is inferred that the transition layer may have consisted of Ag_2O grains, amorphous Ag_2O and a small amount of Al [28]. According to Fig. 8 (f), there were three elements, Ag, O and Al, in the transition layer. Due to the introduction of ultrasonic vibration, the number of dislocations in the system increased and accumulated, so that the compound in the system was in an unstable state, the atom was in an active state, and it was easier to separate from its original equilibrium position, which led to the emergence of a local small range of amorphous structures.

Fig. 9 shows the EBSD test diagram of the ultrasonic assisted solid phase diffusion welding in Al/Ag/Al joints. The sample area selected for EBSD is like that selected for the transmission sample, which included the intermediate layer Ag, base metal 2024Al and intermetallic compound. As shown in Fig. 9 (a), fine grains with different orientations appeared at the interface between Ag_2Al and Al, indicating that grain refinement occurred at the interface between the intermediate layer and the base metal. As shown in Fig. 9 (b), red indicates the deformed grain region, blue corresponds to the recrystallized grain region, and yellow shows the undeformed recrystallized grain region. The diagram shows that red deformed grains accounted for approximately 50%, blue recrystallized grains accounted for approximately 24%, and yellow undeformed recrystallized grains accounted for approximately 26% of the whole joint. The red deformed grains were mainly concentrated in the middle layer Ag and the base metal Al side. Combined with previous analysis, many dislocations and twins appeared in the joint, indicating that plastic deformation occurred in solid metal materials during welding. When solid metal deforms, the oxide film on the surface of the metal material is squeezed and deformed, resulting in rupture. Pure metals are exposed and come into close contact with each other. With the promotion of ultrasonic diffusion, the mutual diffusion between elements is accelerated, thus forming an effective joining.

Fig. 10 (a) shows the mechanical strength diagram of the welded joint for different ultrasonic vibration times. The figure shows that the

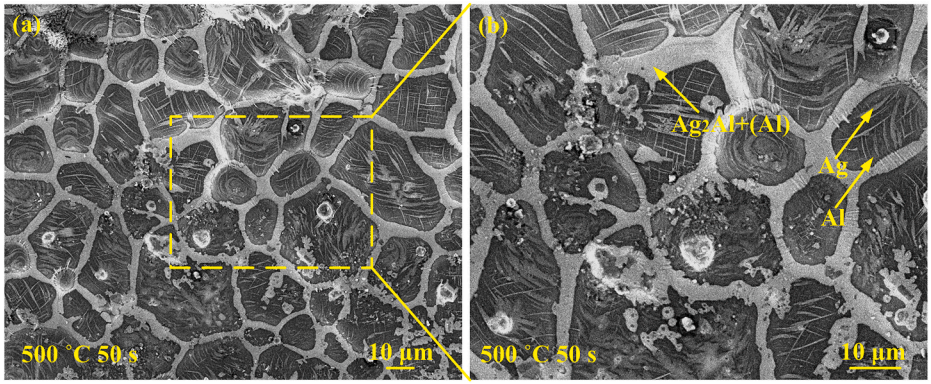

Fig. 11. Fracture morphology of welded joint under ultrasonic vibration for 65 s.

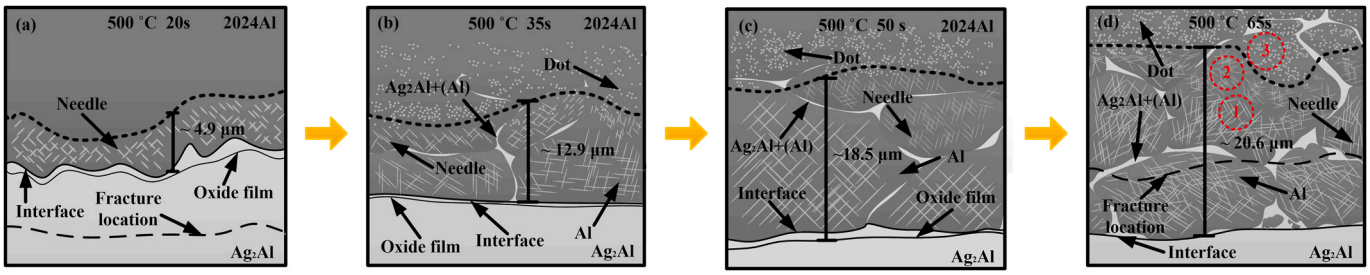

Fig. 12. Schematic diagram of 2024Al side microstructure change under different ultrasonic effects: (a) 20s, (b) 35S, (c) 50s, (d) 60s.

strength of welded joints first increased and then decreased with increasing ultrasonic vibration time. When the ultrasonic vibration time was 50 s, the strength of the welded joint reached the maximum value of 84.33 MPa. Fig. 10 (b) is the fracture XRD test diagram of the welded joint for ultrasonic vibration times of 20 s and 65 s. The figure shows that there was a brittle intermetallic compound, Ag_2Al, in the fracture after ultrasonic vibration for 20 s, which indicates that fracture occurred on the side of the brittle intermetallic compound Ag_2Al. Only Al was detected in the fracture surface after ultrasonic vibration for 65 s. Combined with the fracture morphology, it can be observed that the fracture occurred at the acicular solid solution on the Al side. This shows that with increasing ultrasonic vibration time, the shear strength of welded joints first increased and then decreased, and the fracture position changed from intermetallic Ag_2Al to a needle-like diffusion layer on the Al side. Fig. 10 (c) shows the fracture morphology of the welded joint obtained when the ultrasonic vibration time was 20 s. The figure shows that the fracture mostly had a tongue-like pattern, which characterises brittle fracture. Fig. 10 (d) shows the fracture morphology of welded joints obtained by ultrasonic vibration for 65 s. The figure shows that there were many dimples in the fracture, which was ductile fracture. This shows that with increasing ultrasonic vibration time, the fracture mode changed from brittle fracture to ductile fracture. Fig. 10 (e) shows the amplification diagram of the fracture morphology of the welded joint obtained by applying ultrasonic vibration for 65 s. The grey matter in the gaps between the ellipsoidal blocks of 2024Al was Ag_2Al + (Al). There are a lot of solid solution (Al) and many needles in the fracture, and fracture occurred at the diffusion layer of the needles. According to the analysis of the grey-white needles at the fracture, the Ag content was 58.26 at %, and the Al content was 41.74 at %. Combined with Figs. 5 (c) and Fig. 10 (e), the grey-white needles were Ag_2Al + (Al).

Fig. 11 shows the fracture morphology of the welded joint under ultrasonic vibration for 65 s. The figure shows that many ellipsoidal Al lumps were dispersed in the dimple-like fracture morphology. The grey material filled the gap between the lumps, and the grey-white needles were dispersed in the lumps. Combined with the previous component analysis, the interstitial filler and grey-white needles were Ag_2Al + (Al), and the ellipsoidal block was Al.

Fig. 12 shows a schematic diagram of changes on the 2024 side for different ultrasound effects. The figure shows that with increasing ultrasonication time, Ag in the intermediate layer gradually diffused outward from the grain boundaries, and 2024Al formed several ellipsoidal lumps. The grey phase material filled the interstices between the blocks. The grey phase material was determined to be Ag_2Al + (Al) by EDS. At the same time, there were grey needle-like and grey point-like particles on the 2024Al side. Fig. 12 (d) shows that with increasing distance from the reaction interface, the grey-white needles gradually decrease and shorten, forming grey-white dots, until they disappear completely. According to the combined analysis in Figs. 5 (c) and Fig. 10 (e), the grey-white needle-like substance and grey-white phase substance were both Ag_2Al + (Al). Combining the fracture morphology and XRD diagram shown in Fig. 9 indicates that the intermetallic compounds Ag_2Al and (Al) were present at the fracture position of the welded joint shown in Fig. 11 (a) and (d), respectively.

5. Conclusion

In this paper, the ultrasonic assisted solid phase diffusion welding was successfully applied to join 2024Al by filling with Ag at 500 °C in air. The shear strength of the joint for the ultrasonic times of 50 s was 84.33 MPa, and the fracture occurs at the solid solution layer. Two compounds with different crystal structures appeared in the weld, and it was found that the oxide Ag2O helped the effective joining of the two compounds. Dislocations and twins were observed in the weld, which indicated that plastic deformation had occurred. Combined with the model analysis, the results show that the ultrasonic energy field can optimize the welding process, reduce the welding pressure and shorten the welding time, and the ultrasonic vibration can promote the plastic deformation of metal materials. According to the calculated results of diffusion coefficient, it can be known that ultrasonic vibration can promote the mutual diffusion of elements.

This paper provides a new and efficient welding process suitable for most metal materials.

CRediT authorship contribution statement

Qian Wang: Conceptualization, Supervision, Funding acquisition, Methodology, Project administration. **Yong Nie:** Data curation, Writing – original draft, Writing – review & editing, Investigation. **Yingfeng Shao:** Software. **Hongzhi Liu:** Validation. **Xiaoqiang Hu:** Formal analysis. **Dianzhong Li:** Resources.

Declaration of competing interest

The authors declare that they have no known competing financial interests or personal relationships that could have appeared to influence the work reported in this paper.

Acknowledgments

This research was sponsored by the National Natural Science Foundation of China (Grant No. 51504165).

References

[1] Z.Y. Cai, C. Zhang, R.C. Wang, C.Q. Peng, et al., High-temperature mechanical properties and thermal cycling stability of Al-50Si alloy for electronic packaging, Mater. Sci. Eng., A. 728 (2018) 95–101.
[2] S.W. Fu, C.C. Lee, New solid-state die-attach method using silver foil bonded on aluminum substrate by eutectic reaction, J. Alloys Compd. 774 (2019) 1207–1215.
[3] P. Gaiser, M. Klingler, J. Wilde, The influence of strain hardening of copper on the crack path in Cu/Al2O3/Cu direct bonded copper substrates, Int. J. Fatig. 140 (2020) 105821.
[4] S.S. Akhtar, K.T. Lemboye, A.F.M. Arif, K.S. Al-Athel, Design and performance evaluation of Al2O3-SiC composite for direct-bonded copper substrate, J. Mater. Eng. Perform. 27 (2018) 5831–5844.
[5] V. Moutarlier, R. Viennet, M.P. Gigandet, J.Y. Hihn, Use of ultrasound irradiation during acid etching of the 2024 aluminum alloy: effect on corrosion resistance after anodization, Ultrason. Sonochem. 64 (2020) 104879.
[6] Q.Y. Miao, D.J. Wu, D.S. Chai, Y. Zhan, et al., Comparative study of microstructure evaluation and mechanical properties of 4043 aluminum alloy fabricated by wire-based additive manufacturing, Mater. Des. 186 (2020) 108205.

[7] Z.A. Zhu, Y.Q. Chen, A.A. Luo, L.H. Liu, First conductive atomic force microscopy investigation on the oxide-film removal mechanism by chloride fluxes in aluminum brazing, Scripta Mater. 138 (2017) 12–16.
[8] W.B. Guo, T.M. Luan, J.S. He, J.C. Yan, Ultrasonic-assisted soldering of fine-grained 7034 aluminum alloy using Sn-Zn solders below 300 °C, Ultrason. Sonochem. 40 (2018) 815–821.
[9] S. Kraft, A. Schletz, M. Maerz, Reliability of silver sintering on DBC and DBA substrates for power electronic applications, in: Proceedings of the Integrated Power Electronics Systems (CIPS) 7th International Conference on, 2012, pp. 1–6.
[10] A.H. Assari, B. Eghbali, Solid state diffusion bonding characteristics at the interfaces of Ti and Al layers, J. Alloys Compd. 773 (2019) 50–58.
[11] H. Nami, A. Halvaee, H. Adgi, A. Hadian, Microstructure and mechanical properties of diffusion bonded Al/Mg2Si metal matrix in situ composite, Mater. Des. 31 (2010) 3908–3914.
[12] K.K. Chen, Y.S. Zhang, H.Z. Wang, Effect of acoustic softening on the thermal-mechanical process of ultrasonic welding, Ultrasonics 75 (2017) 9–21.
[13] C.J. Wang, Y. Liu, B. Guo, D.B. Shan, et al., Acoustic softening and stress superposition in ultrasonic vibration assisted uniaxial tension of copper foil: experiments and modeling, Mater. Des. 112 (2016) 246–253.
[14] S.S. Lim, P.L. Rossiter, J.E. Tibballs, Assessment of the Al-Ag binary phase diagram, Calphad 19 (1995) 131–141.
[15] S.W. Fu, C.C. Lee, A study on intermetallic compound formation in Ag–Al system and evaluation of its mechanical properties by micro-indentation, J. Mater. Sci. Mater. Electron. 29 (2018) 3985–3991.
[16] J. Liu, B. Cao, J.W. Yang, Effects of vibration amplitude on microstructure evolution and mechanical strength of ultrasonic spot welded Cu/Al joints, Metals 7 (2017) 471.
[17] Y. Toshimi, T. Junzo, Y. Hiroyoshi, Reaction-diffusion in the Al-Ag system, J. Jpn. Inst. Metals 25 (1975) 167–172.
[18] Callister, Fundamentals of Materials Science and Engineering[M], John Wiley and Sons Ltd, 2004.
[19] D. Finkenstadt, D.D. Johnson, Solute/defect-mediated pathway for rapid nanoprecipitation in solid solutions: γ surface analysis in fcc Al-Ag, Phys. Rev. B 73 (2006), 024101.
[20] H. Paul, J.H. Driver, C. Maurice, A. Piatkowski, The role of shear banding on deformation texture in low stacking fault energy metals as characterized on model Ag crystals, Acta Mater. 55 (2007) 575–588.
[21] L.E. Murr, Interfacial Phenomena in Metals and Alloys S, Addison-Wesley, Reading (MA), 1975, p. 376.
[22] T. Morikawa, K. Higashida, Deformation microstructure and texture in a cold-rolled austenitic steel with low stacking-fault energy, Mater. Trans. 51 (2010) 620–624.
[23] H. Sedaghat, W. Xu, L. Zhang, Ultrasonic vibration-assisted metal forming: constitutive modelling of acoustoplasticity and applications, J. Mater. Process. Technol. 265 (2019) 122–129.
[24] M. Lagos, C. Retamal, An alternate theoretical approach to solid-state bonding, Scripta Mater. 64 (2011) 402–405.
[25] M. Lagos, C. Retamal, A theoretical approach to finite strain superplasticity and some of its applications, Phys. Scripta 81 (2010), 055601.
[26] B. Derby, E.R. Wallach, Theoretical model for diffusion bonding, Metal Science Journal 16 (1982) 49–56.
[27] R.F. Ma, M.Q. Li, H. Li, W.X. Yu, Modeling of void closure in diffusion bonding process based on dynamic conditions, Sci. China Technol. Sci. 55 (2012) 2420–2431.
[28] Y. Xu, X.R. Ma, J.C. Yan, Evolution of interfacial structures and mechanical performance of sapphire and Sn–9Zn–2Al joints by ultrasound, Int. J. Appl. Ceram. Technol. 16 (2019) 2254–2264.